UC Davis

UC Davis Previously Published Works

Title

NMR Structure of Retinal Guanylate Cyclase Activating Protein 5 (GCAP5) with R22A Mutation That Abolishes Dimerization and Enhances Cyclase Activation

Permalink

https://escholarship.org/uc/item/375566jk

Authors

Cudia, Diana L

Ahoulou, Effibe O

Bej, Aritra

et al.

Publication Date

2024-04-25

DOI

10.1021/acs.biochem.4c00046

Copyright Information

This work is made available under the terms of a Creative Commons Attribution-NonCommercial-NoDerivatives License, available at https://creativecommons.org/licenses/by-nc-nd/4.0/

Peer reviewed

eScholarship.org Powered by the California Digital Library
University of California

Biochemistry

pubs.acs.org/biochemistry Article

NMR Structure of Retinal Guanylate Cyclase Activating Protein 5 (GCAP5) with R22A Mutation That Abolishes Dimerization and Enhances Cyclase Activation

Diana L. Cudia, Effibe O. Ahoulou, Aritra Bej, Annika N. Janssen, Alexander Scholten, Karl-W. Koch, and James B. Ames*

Cite This: https://doi.org/10.1021/acs.biochem.4c00046 Read Online

ACCESS | Metrics & More | Article Recommendations

ABSTRACT: Guanylate cyclase activating protein-5 (GCAP5) in zebrafish photoreceptors promotes the activation of membrane receptor retinal guanylate cyclase (GC-E). Previously, we showed the R22A mutation in GCAP5 (GCAP5^{R22A}) abolishes dimerization of GCAP5 and activates GC-E by more than 3-fold compared to that of wild-type GCAP5 (GCAP5^{WT}). Here, we present ITC, NMR, and functional analysis of GCAP5^{R22A} to understand how R22A causes a decreased dimerization affinity and increased cyclase activation. ITC experiments reveal GCAP5^{R22A} binds a total of 3 Ca^{2+}, including two sites in the nanomolar range followed by a single micromolar site. The two nanomolar sites in GCAP5^{WT} were not detected by ITC, suggesting that R22A may affect the binding of Ca^{2+} to these sites. The NMR-derived structure of GCAP5^{R22A} is overall similar to that of GCAP5^{WT} (RMSD = 2.3 Å), except for local differences near R22A (Q19, W20, Y21, and K23) and an altered orientation of the C-terminal helix near the N-terminal myristate. GCAP5^{R22A} lacks an intermolecular salt bridge between R22 and D71 that may explain the weakened dimerization. We present a structural model of GCAP5 bound to GC-E in which the R22 side-chain contacts exposed hydrophobic residues in GC-E. Cyclase assays suggest that GC-E binds to GCAP5^{R22A} with ∼25% higher affinity compared to GCAP5^{WT}, consistent with more favorable hydrophobic contact by R22A that may help explain the increased cyclase activation.

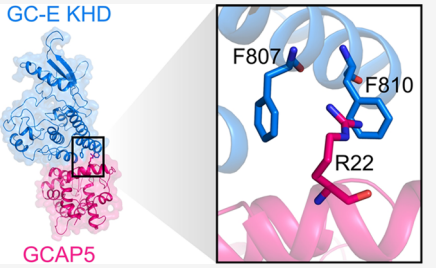

INTRODUCTION

GCAP5,[1−3] an EF-hand Ca^{2+} sensor protein in zebrafish photoreceptor cells, regulates Ca^{2+}-sensitive activation of retinal membrane guanylate cyclase (GC-E[4,5]) that occurs during the recovery phase of visual phototransduction.[6,7] Ca^{2+} binds to the second, third, and fourth EF-hands in GCAP proteins,[8−10] and structures are known for Ca^{2+}-bound forms of GCAP1[9] and GCAP3[11] as well as Ca^{2+}-free forms of GCAP1[12] and GCAP5.[13] Ca^{2+}-bound GCAPs bind to GC-E and inhibit cyclase activity,[14,15] in contrast to Ca^{2+}-free GCAPs that bind to GC-E and activate the cyclase.[14,15] Mutations in GCAP1 that abolish or weaken Ca^{2+} binding cause constitutive activation of GC-E that leads to rod-cone dystrophies.[16−20] NMR,[13,21] EPR-DEER,[13,21] and multiangle light scattering[22] studies indicated that both GCAP1 and GCAP5 form homodimers in solution. Mutations (H19E, Y22E, M26E, F73E, V77E, W94E) that disrupt dimerization of GCAP1[21] also abolish cyclase activation,[23] originally suggesting that dimerization of GCAPs may be essential for the activation of GC-E. However, the R22A mutation in GCAP5 that abolishes dimerization was also shown to cause a 3-fold increase in the activation of GC-E,[13] which demonstrates that GCAP5 dimerization is not essential for promoting cyclase activation. Instead, it seems the dimerization of GCAPs in solution is likely an artifact that occurs in the absence of GC-E because the residues in the dimerization site (H19, Y22, M26, F73, V77, W94) are the same residues that are predicted to bind to GC-E.[23] Fortunately, the Ca^{2+}-free activator form of GCAP5^{R22A} is monomeric under NMR conditions and exhibits very sharp NMR signals[24] (unlike dimeric GCAP1 and GCAP5^{WT}) making it possible to determine an atomic-resolution NMR structure of GCAP5^{R22A} in this study.

We present ITC and NMR analysis of GCAP5^{R22A} along with GC-E cyclase assays to understand how the R22A mutation weakens the dimerization and causes increased cyclase activation. The NMR-derived structure of GCAP5^{R22A} is overall similar to the previous structure of GCAP5^{WT} (RMSD = 2.3 Å). However, small structural differences occur near the mutation site (Q19, W20, Y21, and K23) and in the C-terminal helix (R176, I177, and V178), which alter

Received: January 28, 2024
Revised: April 16, 2024
Accepted: April 17, 2024

Downloaded via UNIV OF CALIFORNIA DAVIS on May 8, 2024 at 22:02:28 (UTC).
See https://pubs.acs.org/sharingguidelines for options on how to legitimately share published articles.

ACS Publications © XXXX American Chemical Society

the environment of exposed hydrophobic residues (H18, Y21, M25, F72, V76, and W93) that interact with GC-E.[23] A structural model of GCAP5 bound to GC-E is presented in which R22 contacts exposed hydrophobic residues in the kinase homology domain (KHD) of GC-E. Thus, the R22A mutation is predicted to enhance binding of GCAP5^{R22A} to GC-E, consistent with cyclase assays that suggest ∼25% higher affinity. The more favorable GC-E interaction with R22A may help explain in part how GCAP5^{R22A} causes enhanced cyclase activation.

MATERIALS AND METHODS

Cloning, Expression, and Purification of GCAP5. Recombinant myristoylated GCAP5^{R22A} (hereafter designated as GCAP5^{R22A}) was used throughout this study and bacterial expression of myristoylated GCAP5^{R22A} was described previously.[13] Cloning of mutants used in this study was similar to that described for other point mutants of GCAPs.[25,26] Purification of GCAP5^{R22A} was performed as described using previous methods.[2]

NMR Spectroscopy. GCAP5^{R22A} samples for NMR experiments consisted of ^{15}N-labeled or ^{15}N/^{13}C-doubly labeled Ca^{2+}-free GCAP5^{R22A} (0.50 mM) dissolved in 5 mM Tris (pH 7.4) buffer containing 2 mM DTT-d_{10}, 1 mM EDTA, 0.04% w/v NaN_3, and 92% H_2O:8% D_2O. All NMR experiments were performed at 37 °C on a Bruker 800 MHz Avance III spectrometer equipped with a triple resonance cryogenic TCI probe and pulsed field gradients. Two-dimensional ^{15}N−^{1}H HSQC and IPAP-HSQC experiments were performed with 2048 (^{1}H) × 256 (^{15}N) data points by using ^{15}N-labeled GCAP5^{R22A}. Three-dimensional NMR HSQC-NOESY and HCCH-TOCSY experiments were performed and analyzed as described previously.[12] Spectra were processed using NMRPipe software package and assigned using SPARKY.[27]

Residual dipolar couplings (RDCs[28]) of GCAP5^{R22A} were measured as described previously.[29] Filamentous bacteriophage Pf1 (Asla Biotech Ltd., Latvia) was used as an orienting medium. Pf1 (12 mg/mL) was added to ^{15}N-labeled GCAP5^{R22A} (0.5 mM) to produce weak alignment. ^{1}H−^{15}N residual dipolar coupling constants (D_{NH}) were measured using a 2D IPAP (inphase/antiphase) ^{1}H−^{15}N HSQC.[30] The backbone N−H RDCs were calculated by measuring the difference in ^{15}N splitting for each amide resonance in both the presence and absence of the orienting medium. The RDC Q-factor and analysis of RDC data were calculated by PALES.[31]

NMR Structure Calculation. NMR-derived structures of GCAP5^{R22A} were calculated using restrained molecular dynamics simulations within Xplor-NIH.[32] Residual dipolar couplings, NOE distances, dihedral angles from TALOS+,[33] and backbone hydrogen bonds were used as structural restraints. NOEs were obtained from ^{15}N-edited NOESY-HSQC and ^{13}C-edited NOESY-HSQC. The Xplor-NIH structure calculation was performed as described for GCAP1.[12] From a total of 200 structures, the 10 lowest-energy structures were deposited in the RCSB PDB (PDB ID: 8VSX). The structure quality was assessed by PROCHECK-NMR[34] and MolProbity.[35]

Isothermal Titration Calorimetry (ITC). ITC experiments were performed using a VP-ITC calorimeter (MicroCal) at 27 °C. The data were acquired and processed with MicroCal software as described previously.[36] The protein samples of GCAP5^{R22A} or GCAP5^{WT} (titrant) were first decalcified by adding 2.0 mM EGTA at pH 7.4. The EGTA was removed by exchanging the decalcified protein samples into 20 mM Tris, 1 mM 2-mercaptoethanol (βME), and 100 mM NaCl. A sample of Ca^{2+} (injectant) was prepared by dissolving it into buffer containing 20 mM Tris (pH 7.4), 1 mM 2-mercaptoethanol (βME), and 100 mM NaCl. The GCAP5^{R22A} (or GCAP5^{WT}) in the sample cell (38 or 45 μM at 25 °C in 1.5 mL) was titrated with aqueous $CaCl_2$ (1.5 or 2.0 mM at 25 °C) using 40 injections of 5 μL each.

Molecular Docking of GC-E (KHD) with GCAP5. The docking of the GC-E kinase homology domain (KHD) with GCAP5 was performed by the web-based docking program HADDOCK 2.4.[37] A modeled structure of KHD (determined by cross-linking/mass spectrometry[38]) was docked with the NMR-derived structure of GCAP5.[13] The missing loops in KHD were modeled using Modeler 9.25 software.[39] Ambiguous interaction restraints (AIRs) in the HADDOCK calculation included exposed hydrophobic residues in KHD (A781, C785, I786, M789, M803, F807, F810) and GCAP5 (H18, Y21, R22, K23, M25, Y36, F72, M73, V76, A77, R92 and W93), which were confirmed experimentally to affect binding.[23,40] The docking calculation generated 500 initial structures using rigid body docking. The best 100 structures were selected for semiflexible simulated annealing followed by water refinement. The structure with the best HADDOCK score from the top cluster indicating the lowest HADDOCK score, RMSD, energy values, and Z-score was selected as the final structure of the KHD/GCAP5 complex. The structure of the mutant GCAP5^{R22A}/KHD complex was generated by mutating the arginine to alanine residue at position 22 using an in-built mutagenesis tool in PyMOL. An energy minimization step in vacuum condition was performed with the GCAP5^{R22A}/KHD complex to minimize steric clashes upon in silico mutation.

Molecular Dynamics (MD) Simulations. MD simulations were performed in duplicate at 37 °C and 1 bar pressure using the GROMACS v2019.6 software package[41] applying CHARMM36 force field[42] for up to 500 ns length. For both wild-type and mutant complexes, the GCAP5/KHD complex was placed in a cubic box, solvated using the TIP3P water model,[43] and neutralized with 150 mM NaCl. The systems were subjected to energy minimization to remove steric clashes using the steepest descent integrator algorithm until the maximum force reached less than 1000 kJ mol^{-1} nm^{-1}, followed by sequential equilibration under NVT and NPT conditions for 1 ns each with a position restraint. Constant temperature and pressure during the simulations were maintained by V-rescale[44] and Parrinello−Rahman[45] algorithms, respectively. Long-range electrostatic interactions were calculated with Particle Mesh Ewald (PME) method,[46] whereas van der Waals and short-range electrostatic interactions were treated with a 12 Å cutoff. All bond lengths were constrained with the LINCS algorithm.[47] Equations of motion were integrated every 2 fs using a leapfrog algorithm.

Data were analyzed using tools integrated with GROMACS software package from trajectories sampled at 10 ps interval, yielding 50,000 structures in each simulation as described previously.[48] Root-mean-square deviation (RMSD) for backbone Cα atom at each time point was obtained using the gmx rmsdist program, and root-mean-square fluctuation (RMSF) was calculated for the Cα atom of each residue using the gmx rmsf tool. The interatomic distance between GCAP5 and KHD as a function of time was calculated using the gmx dist program

https://doi.org/10.1021/acs.biochem.4c00046
Biochemistry XXXX, XXX, XXX−XXX

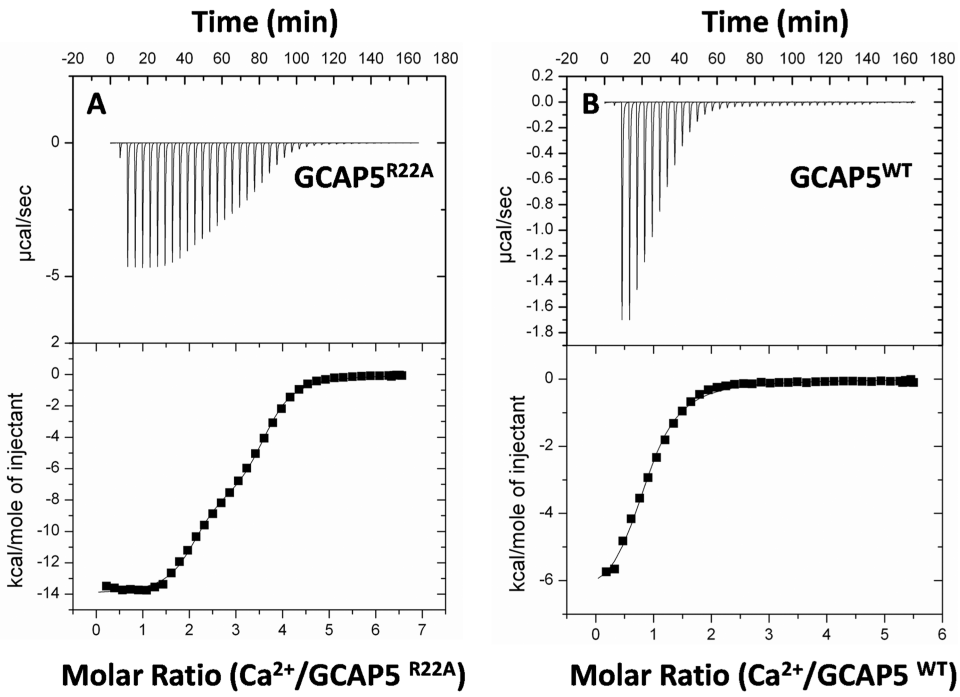

Figure 1. Isothermal titration calorimetry (ITC) analysis of Ca^{2+} binding to $GCAP5^{R22A}$ (A) and $GCAP5^{WT}$ (B). Each isotherm was fit to either a one-site model (solid line in (B)) or two-site model (solid line in (A)) and the binding parameters (N (stoichiometry), K, and ΔH) are given in Table 1. The $GCAP5^{R22A}$ (or $GCAP5^{WT}$) concentrations were 38 μM (or 45 μM) in the sample cell (1.5 mL) for titration with 1.5 mM (or 2.0 mM) Ca^{2+} by using 40 injections of 5 μL each.

Table 1. ITC Ca^{2+} Binding Parameters for $GCAP5^{R22A}$ and $GCAP5^{WT}$[a]

syringe/cell	K (M^{-1})	N	ΔH (kcal/mol)
$Ca^{2+}/GCAP5^{R22A}$[b]	$1.3 \times 10^7 \pm 2.2 \times 10^6$	2.0 ± 0.2	-14.0 ± 0.1
	$3.9 \times 10^5 \pm 4.2 \times 10^4$	1.2 ± 0.2	-7.8 ± 0.4
$Ca^{2+}/GCAP5^{WT}$[c]	$1.6 \times 10^5 \pm 1.2 \times 10^4$	0.9 ± 0.2	-6.9 ± 0.2

[a]Relative errors were estimated from duplicate trials. [b]ITC isotherms fit using a two-site model. [c]ITC isotherms fit using a one-site model.

from the distance of the Cα atom. The average RMSD, RMSF, and Cα-Cα distance values were obtained by taking the arithmetic mean over the duplicate data sets. Cluster analysis of conformers was performed based on the backbone Cα RMSD cutoff of 1.2 Å using the gmx cluster tool, and the center conformation of the largest cluster of each data set was picked as a reference structure for structure analysis.

Guanylate Cyclase Assays. For measuring the EC_{50} values, we reconstituted purified Ca^{2+}-free GCAP5 ($GCAP5^{R22A}$ or $GCAP5^{WT}$) with cell membranes containing heterologously expressed human GC-E (orthologue of bovine and mice RetGC1) in HEK flip 293 cells as described previously.[49,50] Cells were cultivated and harvested by centrifugation (600g, 5 min), the supernatant was discarded, and the pellet was resuspended in 1 mL of 10 mM HEPES/KOH pH 7.4, 1 mM DTT, and 1:500 mammalian protease inhibitor cocktail. Cells were put on ice for 30 min and then disrupted by passing several times through a syringe and put on ice for 30 min again. After incubation, the sample was centrifuged at 13,000g and 4 °C for 5 min. The pellet was resuspended in 100 μL of 50 mM HEPES-KOH at pH 7.4, 50 mM KCl, 20 mM NaCl, 1 mM DTT, and mammalian protease inhibitor cocktail (1:500). The final GCAP5 concentrations were varied between 0.25 μM and 25 μM. Each GCAP5 sample (10 μL) was preincubated with 10 μL of 10 mM K_2H_2EGTA. With 30 s intervals, 10 μL HEK cell membranes containing human GC-E were added to the mixture and incubated for 5 min at RT. 20 μL of 2.5× GC-buffer (75 mM MOPS/KOH pH 7.2, 150 mM KCl, 10 mM NaCl, 8.75 mM $MgCl_2$, 2.5 mM GTP, 0.75 mM ATP, 0.4 mM Zaprinast and 12.5 mM DTT) was added to start the enzyme reaction, and the mixture was incubated for 20 min at 30 °C. The reaction was terminated by adding 50 μL of ice-cold 0.1 mM EDTA and incubated for 5 min at 95 °C. The sample was centrifuged for 10 min at 13,000 rpm and 4 °C before the sample was further processed by HPLC analysis as published before.[26,49] EC_{50} values were extrapolated as the GCAP5 concentration that produced half-maximal cyclase activity and were determined by fitting the saturation curves to a sigmoidal three-parameter model provided by the SigmaPlot 13.0 software.

RESULTS

Isothermal Titration Calorimetry (ITC) Analysis of Ca^{2+} Binding to $GCAP5^{R22A}$. Ca^{2+} binding to $GCAP5^{R22A}$ was monitored by ITC (Figure 1A). The ITC isotherm reveals $GCAP5^{R22A}$ binds a total of 3 Ca^{2+}, and the isotherm looks similar to that observed previously for GCAP1.[10] Two Ca^{2+} atoms bind exothermically to $GCAP5^{R22A}$ in the nanomolar range, and a third Ca^{2+} atom binds with lower affinity in the micromolar range (Table 1). The two nanomolar sites in $GCAP5^{R22A}$ have similar dissociation constants as the Ca^{2+}

https://doi.org/10.1021/acs.biochem.4c00046
Biochemistry XXXX, XXX, XXX−XXX

sites in GCAP1 assigned to EF3 and EF4,[10] suggesting that the nanomolar sites in GCAP5^{R22A} represent Ca^{2+} binding to EF3 and EF4. The lower-affinity site in GCAP5^{R22A} is, therefore, tentatively assigned to EF2. The similar Ca^{2+} binding properties between GCAP5^{R22A} and GCAP1[10] suggest that GCAP5^{R22A} is structurally and functionally intact. The ITC isotherm for binding of Ca^{2+} to GCAP5^{WT} (Figure 1B) detects the binding of only a single Ca^{2+} in the micromolar range and does not detect the two nanomolar sites observed for GCAP5^{R22A}. However, NMR spectra of GCAP5^{WT} indicate a total of three Ca^{2+} bound to GCAP5^{WT} at saturation.[2] Therefore, it is possible that two of the sites in GCAP5^{WT} might already have Ca^{2+} bound before the ITC titration in Figure 1B (caused by high affinity prebinding to background Ca^{2+}), and perhaps explain a lack of ITC heat signal from these two sites during the titration. It is also possible that two of the Ca^{2+} sites in GCAP5^{WT} may have ΔH values that are too low to be detected by ITC.

NMR Spectroscopy of GCAP5^{R22A}. Previous NMR studies on GCAP5^{WT} revealed the wild-type protein is a dimer in solution.[2] The atomic-level structure of Ca^{2+}-free/Mg^{2+}-bound GCAP5^{WT} (called the activator form) was determined previously using a combination of NMR and EPR-DEER.[13] In the current study, we initially wanted to determine the NMR structure of Ca^{2+}-free/Mg^{2+}-bound GCAP5^{R22A} to compare it with the known wild-type structure. However, the $^{15}N-^{1}H$ HSQC spectrum of ^{15}N-labeled Ca^{2+}-free/Mg^{2+}-bound GCAP5^{R22A} displayed peaks with nonuniform intensities and at least 15% of the amide resonances were broadened beyond detection (not shown). The missing NMR peaks for Mg^{2+}-bound GCAP5^{R22A} made it impossible to obtain the complete chemical shift assignments needed for structural analysis. Instead, we discovered that Ca^{2+}-free/Mg^{2+}-free GCAP5^{R22A} apo-state exhibited HSQC spectra (Figure 2, black spectrum) that contained uniform NMR intensities and every amide resonance was detected and assigned.[24] The assigned chemical shifts of Ca^{2+}-free/Mg^{2+}-free GCAP5^{R22A} (hereafter called GCAP5^{R22A}) are similar to the previous chemical shift assignments of Ca^{2+}-free/Mg^{2+}-bound GCAP5^{WT}[51] suggesting that GCAP5^{R22A} (black spectrum in Figure 2) is properly folded and structurally similar to the Ca^{2+}-free/Mg^{2+}-bound activator form of GCAP5^{WT} (red spectrum in Figure 2). The atomic-level NMR-derived structure of GCAP5^{R22A} is described below.

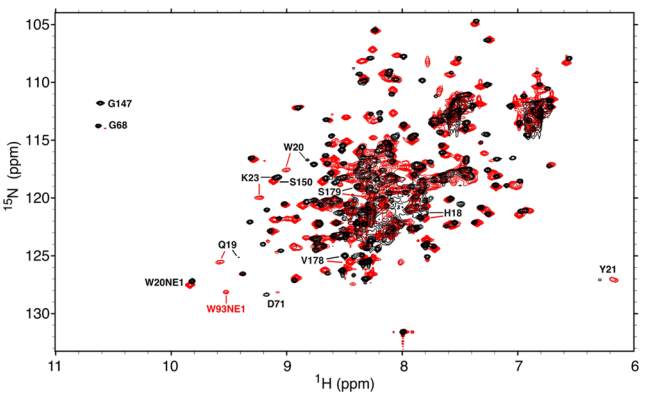

Figure 2. $^{15}N-^{1}H$ HSQC spectra of ^{15}N-labeled apo-state GCAP5^{R22A} (black) and Mg^{2+}-bound GCAP5^{WT} (red). The sharpness of the NMR peaks for GCAP5^{R22A} is consistent with a monomeric structure, in contrast to the broader peaks for dimeric GCAP5^{WT}.

NMR-Derived Structures of GCAP5^{R22A}. NMR chemical shift assignments, published previously for GCAP5^{R22A},[24] were used in this study to determine NOESY-based distances, NMR-derived dihedral angle restraints, and residual dipolar coupling (RDC) restraints (Figure 3A,B) that served as input for restrained molecular dynamics structure calculations (see the Materials and Methods section). RDC magnitude and rhombicity were calculated by fitting the measured RDCs to the calculated structure using the PALES program.[31] The RDC-refined structures have a Q-factor of 0.32 and an R-factor of 0.950 (Figure 3C). The NMR-derived structure of GCAP5^{R22A} (PDB ID: 8VSX) was validated with PROCHECK: 90% of residues belonged to the most favorable region in the Ramachandran plot.

The final NMR structures of GCAP5^{R22A} have a backbone RMSD of 1.2 Å (overlaid in Figure 4A) and structural statistics are given in Table 2. The GCAP5 main-chain structure (Figure 4B,C) contains secondary structure elements identical to those reported previously for GCAP5^{WT}.[13] The overlaid main-chain structures of GCAP5^{R22A} and GCAP5^{WT} have a backbone RMSD of 2.3 Å (Figure 4D). The NMR structure of GCAP5^{R22A} contains two separate domains: N-terminal domain formed by the N-terminal helix (α1), EF1 (residues 18−41), and EF2 (residues 50−82); and C-terminal domain formed by EF3 (residues 87−120), EF4 (residues 129−160), and C-terminal helices (α10 and α11 in Figure 4B,C). The two C-terminal helices (α10 and α11) serve as a linker that connects the N-terminal myristoyl group (magenta in Figure 4B) with EF-hand Ca^{2+}-binding sites (EF3 and EF4) and provides a structural basis for a Ca^{2+} switch mechanism, termed Ca^{2+}-myristoyl tug.[52] The α10 helix has the same structure in both GCAP5^{R22A} and GCAP5^{WT}. However, the α11 helix (residues 174−181) adopts an altered orientation in GCAP5^{R22A} compared to that of GCAP5^{WT} (see red helix in Figure 4C), which explains how the R22A mutation affects the amide chemical shifts of residues in α11.[24] The R22A mutation causes α11 to move closer to the N-terminal myristoyl group (C_{14} methyl is 9.0 Å vs 12.4 Å away from I181 Cα in GCAP5^{R22A} vs GCAP5^{WT}). This movement of α11 causes the Cα atom of N180 (in α11) to move closer to the Cα of I121 (6.2 Å for R22A vs 9.9 Å for WT, orange arrow in Figure 4C). We propose that the altered orientation of the C-terminal helix (orange arrow in Figure 4C) might contribute to the enhanced cyclase activity caused by R22A.

Structural Model of GCAP5 Binding to GC-E. Molecular docking and molecular dynamics simulations were used to generate an atomic-level structural model of GCAP5 bound to GC-E. Previous reports suggest that GC-E contains a kinase homology domain (bovine GC-E residues 537−816, called KHD) that interacts with GCAP proteins.[53,54] A three-dimensional structural model of KHD was previously generated by cross-linking/mass spectrometry (XL-MS) and computational modeling[38] (Figure 5A, blue). The structural model of KHD (Figure 5A, blue) and NMR structure of GCAP5^{WT}[13] were then used as template structures for molecular docking using HADDOCK.[55] Ambiguous interaction restraints (called AIRs) are amino acid residues in the binding site that serve as passive restraints to guide the docking calculation. Previous mutagenesis studies[23] revealed exposed residues in GCAP1 (H18, Y21, R22, K23, M25, Y36, F72, M73, V76, A77, R92, and W93, highlighted red in Figure 4B)

https://doi.org/10.1021/acs.biochem.4c00046
Biochemistry XXXX, XXX, XXX−XXX

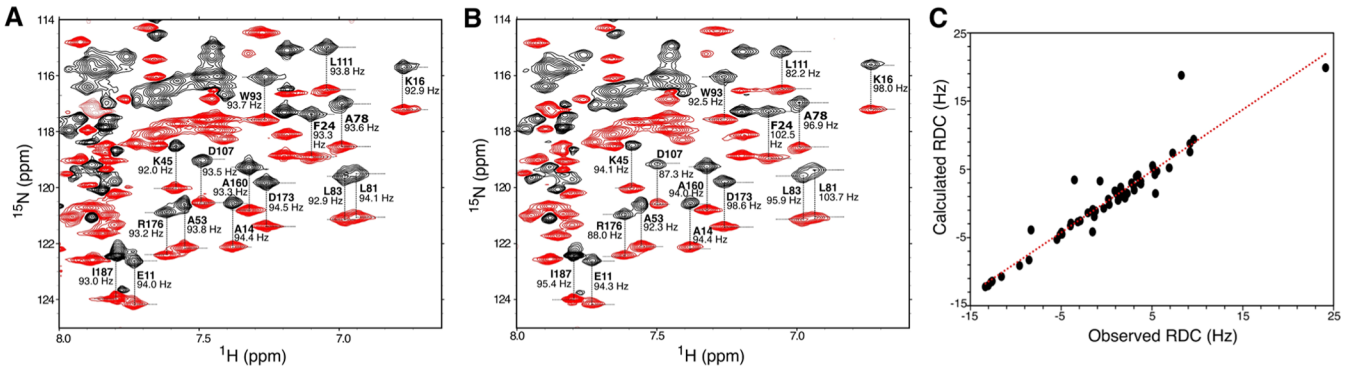

Figure 3. Residual dipolar coupling (RDC) structural analysis of GCAP5^{R22A}. ^{1}H−^{15}N IPAP-HSQC spectra of GCAP5^{R22A} in the absence (A) and presence (B) of 12 mg/mL Pf1 phage. Observed spectral splitting in the absence of Pf1 (J_{NH}) and presence of Pf1 (J_{NH} + D_{NH}) are marked by vertical lines, and their difference was used to calculate RDCs as described in the Materials and Methods section. (C) RDCs calculated from the structure of GCAP5^{R22A} in Figure 4 are plotted vs the RDCs measured in (A) and (B), and show good agreement (Q-factor = 0.32 and an R-factor = 0.950[31]).

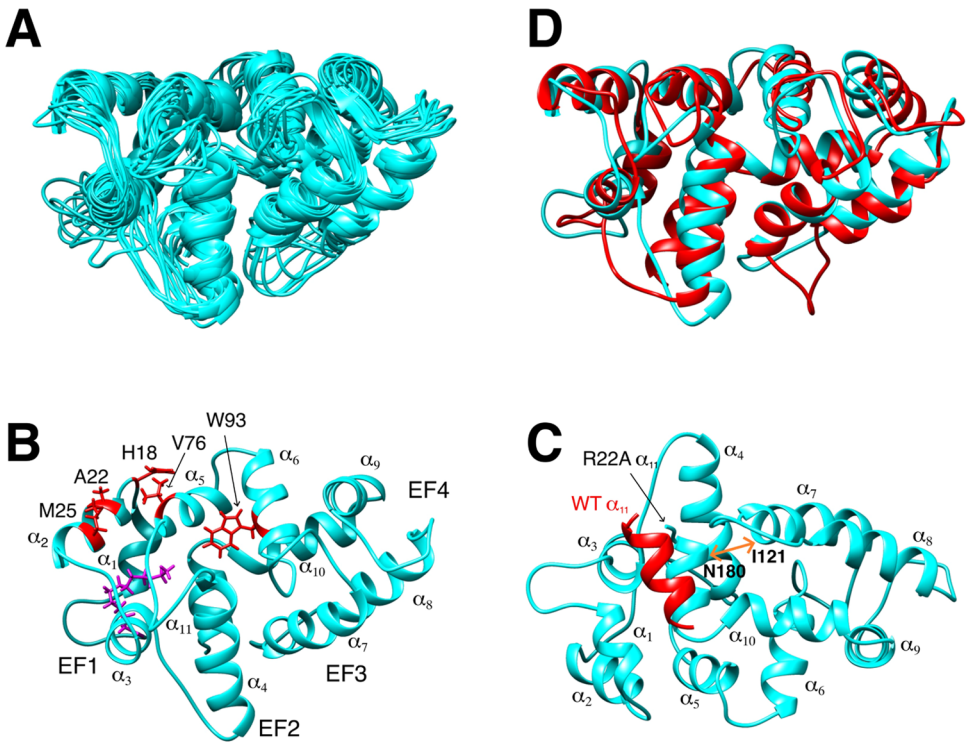

Figure 4. NMR-derived structures of GCAP5^{R22A} (PDB ID: 8VSX). (A) Ensemble of 10 lowest-energy NMR structures. Structural statistics are given in Table 2. (B) Energy-minimized average main-chain structure showing exposed hydrophobic residues (red) and a myristoyl group (magenta). EF-hands and helices are labeled. (C) Back side of GCAP5^{R22A} (rotated 180° from B) showing an altered orientation of α11 caused by R22A (α11 helix from GCAP5^{WT} shown in red) and Cα distance between N180 and I121 shown by orange arrow. (D) Overlay of main-chain structures of GCAP5^{R22A} (cyan) and GCAP5^{WT} (red).

that interact with GC-E and were included as AIRs. The structure of KHD (Figure 5A, blue) suggests a cluster of exposed hydrophobic residues (A781, C785, I786, M789, M803, F807, and F810) that may interact with GCAP5 and were also included as AIRs. Some of these KHD residues (C785 and M789) were verified experimentally to interact with GCAP1.[54,56] An initial docking calculation produced a structure of GCAP5^{WT} bound to KHD (Figure 5A) in which exposed hydrophobic residues in GCAP5 (H18, R22, M25, F72, M73, V76, A77, and W93) contact KHD residues A781, C785, M789, M803, F807, F810, and I813. The KHD residues that contact GCAP5 are all highly conserved in vertebrate homologues of GC-E (Figure 5B). In the docked structure of GCAP5 bound to KHD (Figure 5A), GCAP5 residue R22 is forced to interact with hydrophobic KHD residues (F807 and F810). This unfavorable interaction suggests that the R22A mutation may promote more favorable binding of GCAP5 to GC-E, which may explain the enhanced cyclase activity.

To test the structural effect of R22A predicted by our model (Figure 5), we performed molecular dynamics (MD) simulations on the docked structures of both GCAP5^{R22A}/KHD and GCAP5^{WT}/KHD (Figure 6). The MD simulations showed clear dynamical differences in the final equilibrated structures of GCAP5^{WT}/KHD and GCAP5^{R22A}/KHD. The average root-mean-square deviation (RMSD) of all atoms in KHD bound to GCAP5^{WT} (RMSD = 8 Å in Figure 6A,B) is

https://doi.org/10.1021/acs.biochem.4c00046
Biochemistry XXXX, XXX, XXX−XXX

Table 2. NMR Structural Statistics for GCAP5^{R22A}

NMR restraints	value (restraint violation)
short-range NOEs	430 (0.0 ± 0.0)
long-range NOEs	282 (0.0 ± 0.0)
hydrogen bonds	126 (not used in water refinement)
dihedral angles	230 (0.1 ± 0.3)
$^1D_{HN}$ RDC	57 (0.0 ± 0.0)
RDC Q-factor	0.315
coordinate precision (Å)[a]	
RMSD backbone atoms	1.2 ± 0.002
RMSD all heavy atoms	1.9 ± 0.04
deviation from idealized geometry	
bonds (Å)	0.007 ± 0.001
angles (deg)	0.823 ± 0.015
impropers (deg)	0.925 ± 0.025
Ramachandran plot (%)	
favored region	85.5
allowed region	8.7
outlier region	5.8
structure quality[b]	
clash score	103
Ramachandran outliers	5.9%
side-chain outliers	8.6%

[a]Coordinate precision was calculated for residues 9−16, 20−41, 49−81, 89−120, 130−139, and 148−160. [b]Structure quality metrics assessed by MolProbity.[35]

somewhat larger than that bound to GCAP5^{R22A} (RMSD = 6.5 Å in Figure 6B,6D). The reduced RMSD for GCAP5^{R22A}/KHD suggests that KHD is more stably bound to GCAP5^{R22A} than to GCAP5^{WT}. The structural model of GCAP5 bound to KHD suggests that the C-terminal helix in KHD (residues 800−816) interacts with exposed residues in GCAP5 near the R22A mutation (Figure 6E,F). The intermolecular Cα distances between the KHD C-terminal helix (F807, F810, I813) and exposed residues in GCAP5 (Y21, R22, and M25) are smaller for GCAP5^{R22A} (Figure 6H) than for GCAP5^{WT} (Figure 6G). These shorter intermolecular distances in GCAP5^{R22A}/KHD are most striking for F807 (KHD) and A22 from GCAP5 (6.6 Å for GCAP5^{R22A} vs 10.6 Å for GCAP5^{WT}), F810 (KHD) and M25 (6.4 Å for GCAP5^{R22A} vs 10 Å for GCAP5^{WT}), and I813 (KHD) and M25 (8.9 Å for GCAP5^{R22A} vs 13.7 Å for GCAP5^{WT}). These observations (Figure 6G,H) together with the RMSD analysis (Figure 6A−D) suggest that the GCAP5/KHD mutant complex is stabilized by the increased hydrophobic contact caused by R22A. The results predict that GC-E should bind to GCAP5^{R22A} with higher affinity than that it binds to GCAP5^{WT}.

Guanylate Cyclase Assays Monitor GC-E Binding to GCAP5^{R22A} vs GCAP5^{WT}. Our structural model of GCAP5 binding to GC-E (Figures 5 and 6) suggests that the R22 side-chain contacts exposed hydrophobic residues in GC-E and the R22A mutation might enhance the binding to GC-E. To test this hypothesis and monitor the binding of GCAP5 to GC-E, we measured guanylate cyclase enzymatic activity as a function of added GCAP5 (Figure 7). The concentration of GCAP5 that produces half-maximal cyclase activity (called EC_{50}) is proportional to the binding dissociation constant (K_D = [GCAP5][GC-E]/[GC-E:GCAP5]). The measured EC_{50} values from different sample preparations yielded an EC_{50} = 8 ± 4 μM for GCAP5^{R22A} (n = 14) vs EC_{50} = 11 ± 5 μM for GCAP5^{WT} (n = 9). Although data sets were quite variable, representative plots (Figure 7) illustrate a slightly lower EC_{50} for GCAP5^{R22A}. On average, the EC_{50} for GCAP5^{R22A} was at least 25% smaller than that for GCAP5^{WT}, but the standard deviation in EC_{50} is larger than the average difference of EC_{50} for GCAP5^{R22A} vs GCAP5^{WT}. The large variability may be explained by variable levels of recombinant GC-E in the different cell preparations that was also seen in different maximal GC activities at saturating GCAP5 concentrations. We calculated the ratio (R22A/WT) of relative maximal cyclase activity and EC_{50} values for each cell preparation and obtained mean ratios of 1.35 ± 0.5 and 0.83 ± 0.1, respectively. Routinely, we tested for sufficient GC-E expression in HEK cells by testing the activity in the presence of human GCAP1 yielding for example 0.17 nmol × min^{-1} × mg^{-1} cGMP at 33 μM Ca^{2+} and 11 nmol × min^{-1} × mg^{-1} cGMP at low Ca^{2+} (EGTA), which agrees with previous determinations.[49,50] The range of EC_{50} values for GCAP5^{R22A} (EC_{50} = 1.6−15.6 μM, n = 14) was similar to that of GCAP5^{WT} (EC_{50} = 3.7−16.2 μM, n = 9), but the shifted range suggests that GCAP5^{R22A} has a smaller EC_{50}. Future studies are needed to reduce the variability in the EC_{50} measurement and more accurately verify whether the EC_{50} is smaller for GCAP5^{R22A}.

DISCUSSION

We present ITC Ca^{2+} binding data (Figure 1), the NMR structure of GCAP5^{R22A} (Figures 2−4), guanylate cyclase assays (Figure 7), and a structural model of GCAP5 bound to GC-E (Figures 5 and 6) to help understand how the R22A mutation enhances cyclase activation. The ITC data demonstrate that GCAP5^{R22A} binds a total of 3 Ca^{2+} with a binding isotherm (Figure 1A) similar to that of GCAP1.[10] Surprisingly, the ITC data for GCAP5^{WT} detected the binding of only one Ca^{2+}. We suggest that the two missing sites in GCAP5^{WT} might be explained if these sites were inadvertently prebound with Ca^{2+} before the titration. Alternatively, the two Ca^{2+} sites in GCAP5^{WT} may have ΔH values that are too low to detect by ITC. In any event, the different ITC isotherms for Ca^{2+} binding to GCAP5^{WT} vs GCAP5^{R22A} may correlate with the higher cyclase activation caused by the R22A mutation.[13] Indeed, the ITC isotherm for Ca^{2+} binding to GCAP5^{R22A} is very similar to that of GCAP1, and both GCAP5^{R22A} and GCAP1 cause a similar high degree of cyclase activation in contrast to the lower cyclase activation by GCAP5^{WT}.

The NMR structure of GCAP5^{R22A} looks similar to that of GCAP5^{WT}[13] (Figure 4D). The main structural difference is concentrated in a local region near the R22A mutation (residues Q19, W20, Y21, and K23). Also, the C-terminal helix (α11) is oriented differently in GCAP5^{R22A} compared to GCAP5^{WT} (see red helix and orange arrow in Figure 4C). The R22A mutation causes α11 to move closer to the N-terminal myristoyl group (magenta in Figure 4B), which may explain how R22A causes enhanced cyclase activation. The shorter distance between α11 and the myristate in GCAP5^{R22A} might more effectively couple the N-terminal myristoyl group to Ca^{2+}-dependent structural changes in the EF-hands as proposed by the Ca^{2+}-myristoyl tug mechanism.[52] The R22A mutation also disrupts an intermolecular salt bridge between R22 and D71 in the GCAP5 dimer,[13] which could explain how R22A weakens GCAP5 dimerization.[22] We propose that the weakened dimerization of GCAP5^{R22A} could also help cause increased cyclase activation, because dimeric GCAP5^{WT} might

https://doi.org/10.1021/acs.biochem.4c00046
Biochemistry XXXX, XXX, XXX−XXX

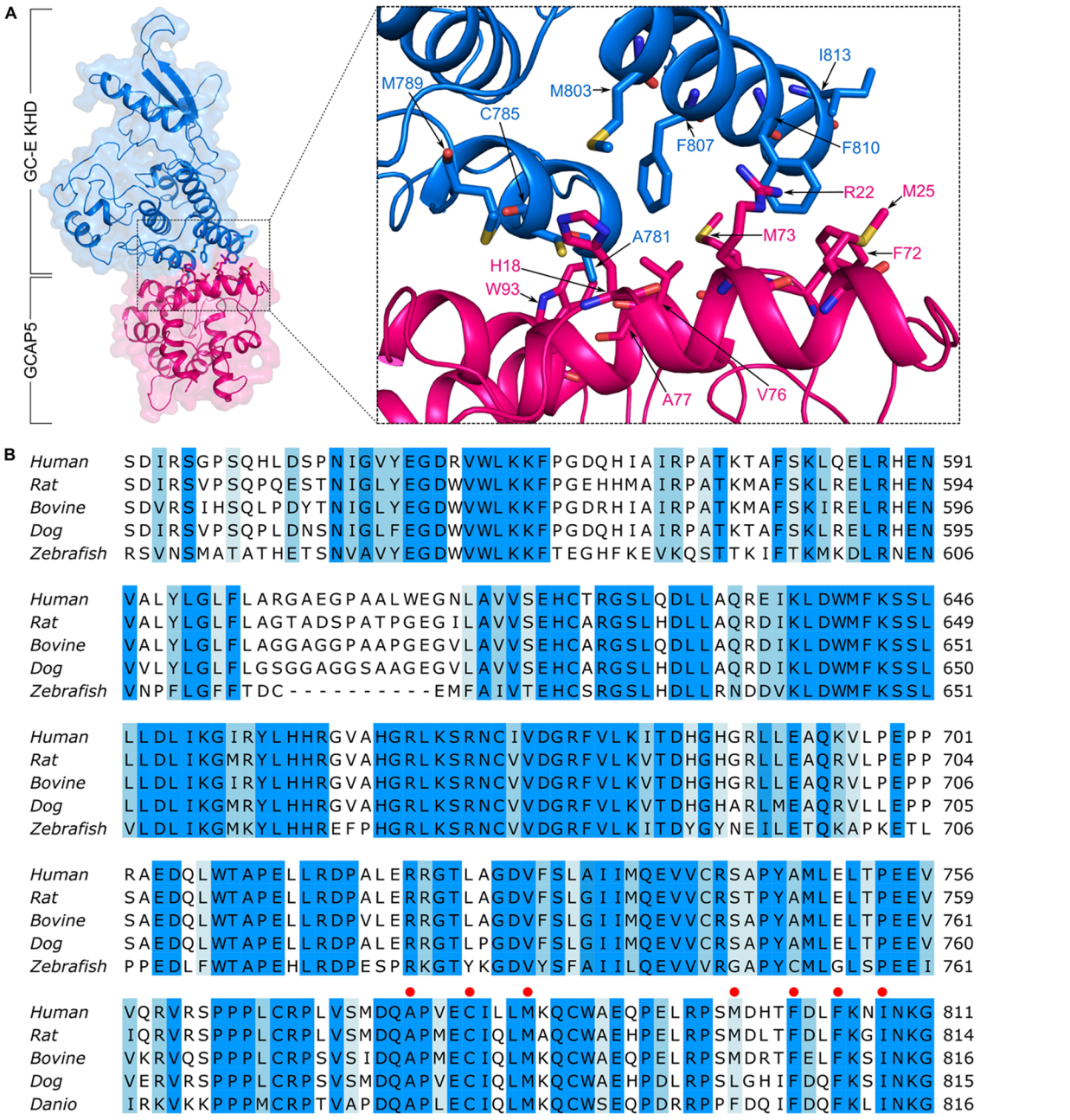

Figure 5. Structural modeling of GCAP5 binding to GC-E. (A) Structural model of KHD (blue) bound to GCAP5 (red) generated by molecular docking. Side-chain atoms of residues involved in the interaction are labeled and indicated as sticks. (B) Multiple sequence alignment of KHD from various vertebrate species of GC-E. Conserved residues located at the binding interface are indicated with red dots.

competitively inhibit the binding of GCAP5 to GC-E (Figure 5A), in contrast to the fully monomeric GCAP5^{R22A}.

The binding of Mg^{2+} to GCAP5 and GCAP1 has different structural effects. The structure of the metal-free apo-state of GCAP5^{R22A} (Mg^{2+}-free/Ca^{2+}-free) presented in this study is very similar to the structure of Mg^{2+}-bound/Ca^{2+}-free GCAP5^{WT} (Figures 2 and 4D). Therefore, the binding of Mg^{2+} to GCAP5 has little effect on its overall structure. This is quite different from previous studies on GCAP1 that showed Mg^{2+} binding to EF2 is essential for forming a functional cyclase activator state.[10,14,57] The apo-state of GCAP1 (Mg^{2+}-free/Ca^{2+}-free) forms a molten globule structure that lacks a stable hydrophobic core,[10] and the binding of Mg^{2+} to GCAP1 is required to form a stable tertiary structure.[10] In short, Mg^{2+}-binding to GCAP1 is essential for forming a stably folded cyclase activator state, in contrast to Ca^{2+}-free GCAP5 that forms a stably folded structure in the absence of Mg^{2+} (Figure 4).

A structural model of GCAP5 bound to GC-E was generated by docking the NMR structure of GCAP5 onto a modeled structure of the GC-E kinase homology domain KHD (Figure 5). The KHD structural model was determined previously using cross-linking/mass spectrometry and computational modeling,[38] which closely matches the KHD structure calculated by structure prediction software, AlphaFold2.[58] The KHD structure has many exposed hydrophobic residues (A781, C785, M789, M803, F807, F810, and I813) that are predicted to contact exposed hydrophobic residues in GCAP5

https://doi.org/10.1021/acs.biochem.4c00046
Biochemistry XXXX, XXX, XXX−XXX

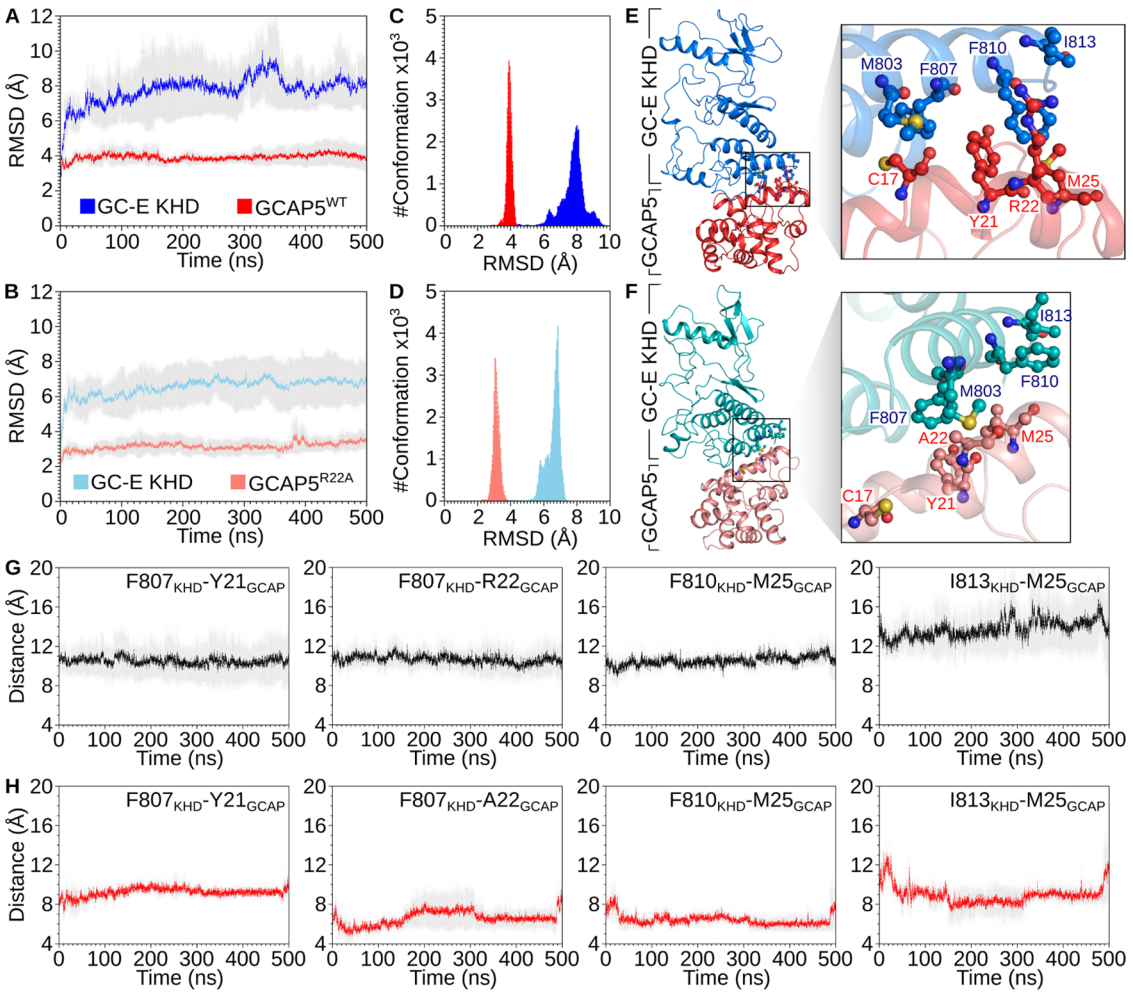

Figure 6. MD simulations of KHD bound to GCAP5. MD simulations showing the average RMSD of all atoms in KHD (blue) and GCAP5 (red) for KHD bound to (A) GCAP5^{WT} and (B) GCAP5^{R22A}. The standard error of the average RMSD (from duplicate simulations) is shaded in gray. RMSD distributions (GCAP5, red; KHD, blue) of KHD bound to (C) GCAP5^{WT} and (D) GCAP5^{R22A}. Equilibrated structures: (E) GCAP5^{WT}/KHD and (F) GCAP5^{R22A}/KHD. Side-chain atoms of residues in the binding site are represented as sticks and labeled. During MD simulations, the intermolecular distance between Cα atoms from KHD (F807, F810, and I813) and GCAP5 (Y21, R22, and M25) are shown as indicated in (G) and (H). The average intermolecular Cα distance for the indicated residues in GCAP5^{WT} (G) and GCAP5^{R22A} (H) are shown by black and red traces, respectively. The standard error of the mean intermolecular distance (from duplicate simulations) is shaded in gray.

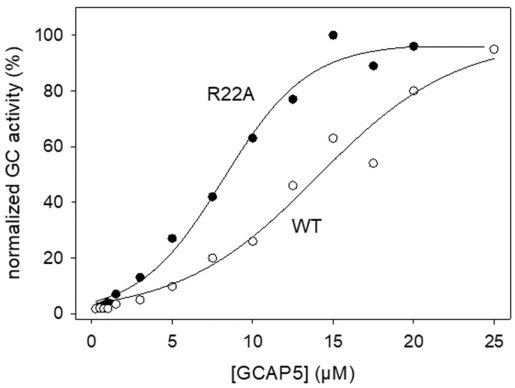

Figure 7. Activation of photoreceptor guanylate cyclase by GCAP5^{R22A} vs GCAP5^{WT}. Normalized enzymatic activity of GC-E plotted as a function of the concentration of GCAP5^{R22A} (filled circles) or GCAP5^{WT} (open circles). Representative titrations yielded EC_{50} values of 8.2 μM (GCAP5^{R22A}) and 14.1 μM (GCAP5^{WT}). The average EC_{50} was determined to be 8 ± 4 μM (n = 14) for GCAP5^{R22A} and 11 ± 5 μM (n = 9) for GCAP5^{WT}.

(H18, Y21, R22, M25, F72, V76, and W93, highlighted red in Figure 4B), and the corresponding residues in GCAP1 were shown to be essential for binding to GC-E.[23] The GCAP5/KHD binding interface places the positively charged R22 side chain in contact with aromatic side chains of F807 and F810 in KHD. This unfavorable R22 side-chain interaction with KHD (Figure 5A) might explain why the R22A mutation causes a more stable binding interaction in the MD simulations (Figure 6) and a lower EC-50 value for cyclase activation by GCAP5^{R22A} (Figure 7). Future cryo-EM structural studies are needed to determine the structure of full-length GC-E bound to GCAP5 to test the predictions of our model (Figure 5A) and more accurately define how GC-E binds to GCAP proteins.

■ ASSOCIATED CONTENT

Accession Codes

Atomic coordinates for GCAP5^{R22A}: 8VSX (PDB).

https://doi.org/10.1021/acs.biochem.4c00046
Biochemistry XXXX, XXX, XXX−XXX

AUTHOR INFORMATION

Corresponding Author

James B. Ames − *Department of Chemistry, University of California, Davis, Davis, California 95616, United States;* orcid.org/0000-0003-0934-2595; Phone: (530) 752-6358; Email: jbames@ucdavis.edu

Authors

Diana L. Cudia − *Department of Chemistry, University of California, Davis, Davis, California 95616, United States*

Effibe O. Ahoulou − *Department of Chemistry, University of California, Davis, Davis, California 95616, United States*

Aritra Bej − *Department of Chemistry, University of California, Davis, Davis, California 95616, United States*

Annika N. Janssen − *Division of Biochemistry, Department of Neuroscience, Carl von Ossietzky Universität Oldenburg, 26129 Oldenburg, Germany*

Alexander Scholten − *Division of Biochemistry, Department of Neuroscience, Carl von Ossietzky Universität Oldenburg, 26129 Oldenburg, Germany*

Karl-W. Koch − *Division of Biochemistry, Department of Neuroscience, Carl von Ossietzky Universität Oldenburg, 26129 Oldenburg, Germany;* orcid.org/0000-0003-1501-0044

Complete contact information is available at: https://pubs.acs.org/10.1021/acs.biochem.4c00046

Author Contributions

J.B.A. designed research and, with input from other authors, wrote the paper; D.L.C., E.O.A., A.B., A.N.J., A.S., K.-W.K., and J.B.A. performed research; D.L.C., E.O.A., A.B., A.S., K.-W.K., and J.B.A. analyzed data.

Notes

The authors declare no competing financial interest.

ACKNOWLEDGMENTS

The authors thank Derrick Kaseman and Ping Yu for help with NMR experiments performed at the UC Davis NMR Facility. This work was supported by NIH grant (R01-EY012347) to J.B.A., and grants from the Deutsche Forschungsgemeinschaft, KO948/15-2 (Project Number 322057463) to K.-W.K. and GRK1885 to K.-W.K. and to the Research Training Group in Oldenburg.

ABBREVIATIONS

GCAP, guanylate cyclase activating protein; GC-E, retinal membrane guanylate cyclase; HSQC, heteronuclear single quantum coherence; ITC, isothermal titration calorimetry; KHD, kinase homology domain; NMR, nuclear magnetic resonance; NOESY, NOE spectroscopy

REFERENCES

(1) Imanishi, Y.; Yang, L.; Sokal, I.; Filipek, S.; Palczewski, K.; Baehr, W. Diversity of guanylate cyclase-activating proteins (GCAPs) in teleost fish: characterization of three novel GCAPs (GCAP4, GCAP5, GCAP7) from zebrafish (Danio rerio) and prediction of eight GCAPs (GCAP1−8) in pufferfish (Fugu rubripes). *J. Mol. Evol.* **2004**, *59*, 204−217.

(2) Lim, S.; Scholten, A.; Manchala, G.; Cudia, D.; Zlomke-Sell, S. K.; Koch, K. W.; Ames, J. B. Structural Characterization of Ferrous Ion Binding to Retinal Guanylate Cyclase Activator Protein 5 from Zebrafish Photoreceptors. *Biochemistry* **2017**, *56*, 6652−6661.

(3) Rätscho, N.; Scholten, A.; Koch, K. W. Expression profiles of three novel sensory guanylate cyclases and guanylate cyclase-activating proteins in the zebrafish retina. *Biochim. Biophys. Acta* **2009**, *1793*, 1110−1114.

(4) Dizhoor, A. M.; Lowe, D. G.; Olsevskaya, E. V.; Laura, R. P.; Hurley, J. B. The human photoreceptor membrane guanylyl cyclase, RetGC, is present in outer segments and is regulated by calcium and a soluble activator. *Neuron* **1994**, *12*, 1345−1352.

(5) Lowe, D. G.; Dizhoor, A. M.; Liu, K.; Gu, Q.; Spencer, M.; Laura, R.; Lu, L.; Hurley, J. B. Cloning and expression of a second photoreceptor-specific membrane retina guanylyl cyclase (RetGC), RetGC-2. *Proc. Natl. Acad. Sci. U.S.A.* **1995**, *92*, 5535−5539.

(6) Koch, K. W.; Duda, T.; Sharma, R. K. Photoreceptor specific guanylate cyclases in vertebrate phototransduction. *Mol. Cell. Biochem.* **2002**, *230*, 97−106.

(7) Koch, K. W.; Stryer, L. Highly cooperative feedback control of retinal rod guanylate cyclase by calcium ions. *Nature* **1988**, *334*, 64−66.

(8) Ames, J. B.; Dizhoor, A. M.; Ikura, M.; Palczewski, K.; Stryer, L. Three-dimensional structure of guanylyl cyclase activating protein-2, a calcium-sensitive modulator of photoreceptor guanylyl cyclases. *J. Biol. Chem.* **1999**, *274*, 19329−19337.

(9) Stephen, R.; Bereta, G.; Golczak, M.; Palczewski, K.; Sousa, M. C. Stabilizing function for myristoyl group revealed by the crystal structure of a neuronal calcium sensor, guanylate cyclase-activating protein 1. *Structure* **2007**, *15*, 1392−1402.

(10) Lim, S.; Peshenko, I. V.; Dizhoor, A. M.; Ames, J. B. Effects of Ca2+, Mg2+, and myristoylation on guanylyl cyclase activating protein 1 structure and stability. *Biochemistry* **2009**, *48*, 850−862.

(11) Stephen, R.; Palczewski, K.; Sousa, M. C. The crystal structure of GCAP3 suggests molecular mechanism of GCAP-linked cone dystrophies. *J. Mol. Biol.* **2006**, *359*, 266−275.

(12) Lim, S.; Peshenko, I. V.; Olshevskaya, E. V.; Dizhoor, A. M.; Ames, J. B. Structure of Guanylyl Cyclase Activator Protein 1 (GCAP1) Mutant V77E in a Ca2+-free/Mg2+-bound Activator State. *J. Biol. Chem.* **2016**, *291*, 4429−4441.

(13) Cudia, D.; Roseman, G. P.; Assafa, T. E.; Shahu, M. K.; Scholten, A.; Menke-Sell, S. K.; Yamada, H.; Koch, K. W.; Milhauser, G.; Ames, J. B. NMR and EPR-DEER Structure of a Dimeric Guanylate Cyclase Activator Protein-5 from Zebrafish Photoreceptors. *Biochemistry* **2021**, *60*, 3058−3070.

(14) Peshenko, I. V.; Dizhoor, A. M. Ca2+ and Mg2+ binding properties of GCAP-1. Evidence that Mg2+-bound form is the physiological activator of photoreceptor guanylyl cyclase. *J. Biol. Chem.* **2006**, *281*, 23830−23841.

(15) Peshenko, I. V.; Dizhoor, A. M. Activation and inhibition of photoreceptor guanylyl cyclase by guanylyl cyclase activating protein 1 (GCAP-1): the functional role of Mg2+/Ca2+ exchange in EF-hand domains. *J. Biol. Chem.* **2007**, *282*, 21645−21652.

(16) Behnen, P.; Dell' Orco, D.; Koch, K. W. Involvement of the calcium sensor GCAP1 in hereditary cone dystrophies. *Biol. Chem.* **2010**, *391*, 631−637.

(17) Dell'Orco, D.; Behnen, P.; Linse, S.; Koch, K. W. Calcium binding, structural stability and guanylate cyclase activation in GCAP1 variants associated with human cone dystrophy. *Cell. Mol. Life Sci.* **2010**, *67*, 973−984.

(18) Payne, A. M.; Downes, S. M.; Bessant, D. A.; Taylor, R.; Holder, G. E.; Warren, M. J.; Bird, A. C.; Bhattacharya, S. S. A mutation in guanylate cyclase activator 1A (GUCA1A) in an autosomal dominant cone dystrophy pedigree mapping to a new locus on chromosome 6p21.1. *Hum. Mol. Genet.* **1998**, *7*, 273−277.

(19) Sokal, I.; Li, N.; Surgucheva, I.; Warren, M. J.; Payne, A. M.; Bhattacharya, S. S.; Baehr, W.; Palczewski, K. GCAP1 (Y99C) mutant is constitutively active in autosomal dominant cone dystrophy. *Mol. Cell* **1998**, *2*, 129−133.

(20) Wilkie, S. E.; Li, Y.; Deery, E. C.; Newbold, R. J.; Garibaldi, D.; Bateman, J. B.; Zhang, H.; Lin, W.; Zack, D. J.; Bhattacharya, S. S.; Warren, M. J.; Hunt, D. M.; Zhang, K. Identification and functional consequences of a new mutation (E155G) in the gene for GCAP1

that causes autosomal dominant cone dystrophy. *Am. J. Hum. Genet.* **2001**, *69*, 471−480.
(21) Lim, S.; Roseman, G.; Peshenko, I.; Manchala, G.; Cudia, D.; Dizhoor, A.; Millhauser, G.; Ames, J. Retinal Guanylyl Cyclase Activating Protein 1 Forms a Functional Dimer. *PLoS One* **2018**, *13*, e0193947.
(22) Boni, F.; Marino, V.; Bidoia, C.; Mastrangelo, E.; Barbiroli, A.; Dell'Orco, D.; Milani, M. Modulation of Guanylate Cyclase Activating Protein 1 (GCAP1) Dimeric Assembly by Ca(2+) or Mg(2+): Hints to Understand Protein Activity. *Biomolecules* **2020**, *10*, 1408.
(23) Peshenko, I. V.; Olshevskaya, E. V.; Lim, S.; Ames, J. B.; Dizhoor, A. M. Identification of target binding site in photoreceptor guanylyl cyclase-activating protein 1 (GCAP1). *J. Biol. Chem.* **2014**, *289*, 10140−10154.
(24) Cudia, D.; Ahoulou, E. O.; Ames, J. B. Chemical shift assignments of retinal guanylyl cyclase activating protein 5 (GCAP5) with a mutation (R22A) that abolishes dimerization and enhances cyclase activation. *Biomol. NMR Assignments* **2023**, *17*, 115−119.
(25) Fries, R.; Scholten, A.; Saftel, W.; Koch, K. W. Operation profile of zebrafish guanylate cyclase-activating protein 3. *J. Neurochem.* **2012**, *121*, 54−65.
(26) Scholten, A.; Koch, K. W. Differential calcium signaling by cone specific guanylate cyclase-activating proteins from the zebrafish retina. *PLoS One* **2011**, *6*, e23117.
(27) Lee, W.; Tonelli, M.; Markley, J. L. NMRFAM-SPARKY: enhanced software for biomolecular NMR spectroscopy. *Bioinformatics* **2015**, *31*, 1325−1327.
(28) Tjandra, N.; Bax, A. Direct measurement of disances and angles in biomolecules by NMR in a dilute liquid crystalline medium. *Science* **1997**, *278*, 1111−1114.
(29) Peshenko, I. V.; Yu, Q.; Lim, S.; Cudia, D.; Dizhoor, A. M.; Ames, J. B. Retinal degeneration 3 (RD3) protein, a retinal guanylyl cyclase regulator, forms a monomeric and elongated four-helix bundle. *J. Biol. Chem.* **2019**, *294*, 2318−2328.
(30) Ottiger, M.; Delaglio, F.; Marquardt, J. L.; Tjandra, N.; Bax, A. Measurement of dipolar couplings for methylene and methyl sites in weakly oriented macromolecules and their use in structure determination. *J. Magn. Reson.* **1998**, *134*, 365−369.
(31) Zweckstetter, M. NMR: prediction of molecular alignment from structure using the PALES software. *Nat. Protoc* **2008**, *3*, 679−690.
(32) Schwieters, C. D.; Kuszewski, J. J.; Tjandra, N.; Clore, G. M. The Xplor-NIH NMR molecular structure determination package. *J. Magn. Reson.* **2003**, *160*, 65−73.
(33) Shen, Y.; Delaglio, F.; Cornilescu, G.; Bax, A. TALOS+: a hybrid method for predicting protein backbone torsion angles from NMR chemical shifts. *J. Biomol. NMR* **2009**, *44*, 213−223.
(34) Laskowski, R. A.; Rullmann, J. A.; MacArthur, M. W.; Kaptein, R.; Thornton, J. M. AQUA and PROCHECK-NMR: programs for checking the quality of protein structures solved by NMR. *J. Biomol. NMR* **1996**, *8*, 477−486.
(35) Chen, V. B.; Arendall, W. B., 3rd; Headd, J. J.; Keedy, D. A.; Immormino, R. M.; Kapral, G. J.; Murray, L. W.; Richardson, J. S.; Richardson, D. C. MolProbity: all-atom structure validation for macromolecular crystallography. *Acta Crystallogr., Sect. D* **2010**, *66*, 12−21.
(36) Wingard, J. N.; Chan, J.; Bosanac, I.; Haeseleer, F.; Palczewski, K.; Ikura, M.; Ames, J. B. Structural analysis of Mg2+ and Ca2+ binding to CaBP1, a neuron-specific regulator of calcium channels. *J. Biol. Chem.* **2005**, *280*, 37461−37470.
(37) van Zundert, G. C.; Rodrigues, J. P.; Trellet, M.; Schmitz, C.; Kastritis, P. L.; Karaca, E.; Melquiond, A. S.; van Dijk, M.; de Vries, S. J.; Bonvin, A. M. The HADDOCK2.2 Web Server: User-Friendly Integrative Modeling of Biomolecular Complexes. *J. Mol. Biol.* **2016**, *428*, 720−725.
(38) Rehkamp, A.; Tanzler, D.; Tuting, C.; Kastritis, P. L.; Iacobucci, C.; Ihling, C. H.; Kipping, M.; Koch, K. W.; Sinz, A. First 3D-Structural Data of Full-Length Guanylyl Cyclase 1 in Rod-Outer-Segment Preparations of Bovine Retina by Cross-Linking/Mass Spectrometry. *J. Mol. Biol.* **2021**, *433*, No. 166947.
(39) Šali, A.; Blundell, T. L. Comparative protein modelling by satisfaction of spatial restraints. *J. Mol. Biol.* **1993**, *234*, 779−815.
(40) Bose, A.; Visweswariah, S. S. The pseudokinase domain in receptor guanylyl cyclases. *Methods Enzymol.* **2022**, *667*, 535−574.
(41) Abraham, M. J.; Murtola, T.; Schulz, R.; Pall, S.; Smith, J. C.; Hess, B.; Lindahl, E. GROMACS: High performance molecular simulations through multi-level parallelism from laptops to supercomputers. *SoftwareX* **2015**, *1−2*, 19−25.
(42) Vanommeslaeghe, K.; Hatcher, E.; Acharya, C.; Kundu, S.; Zhong, S.; Shim, J.; Darian, E.; Guvench, O.; Lopes, P.; Vorobyov, I.; Mackerell, A. D. CHARMM general force field: A force field for drug-like molecules compatible with the CHARMM all-atom additive biological force fields. *J. Comput. Chem.* **2010**, *31*, 671−690.
(43) Jorgensen, W. L.; Chandrasekhar, J.; Madura, J. D.; Impey, R. W.; Klein, M. L. Comparison of simple potential functions for simulating liquid water. *J. Chem. Phys.* **1983**, *79*, 926−935.
(44) Bussi, G.; Donadio, D.; Parrinello, M. Canonical sampling through velocity rescaling. *J. Chem. Phys.* **2007**, *126*, 014101.
(45) Parrinello, M.; Rahman, A. Polymorphic transitions in single crystals: A new molecular dynamics method. *J. Appl. Phys.* **1981**, *52*, 7182−7190.
(46) Darden, T.; York, D.; Pedersen, L. Particle mesh Ewald: An N·log(N) method for Ewald sums in large systems. *J. Chem. Phys.* **1993**, *98*, 010089.
(47) Hess, B.; Bekker, H.; Berendsen, H. J.; Fraaije, J. LINCS: A linear constraint solver for molecular simulations. *J. Comput. Chem.* **1997**, *18*, 1463−1472.
(48) Mozumder, S.; Bej, A.; Sengupta, J. Ligand-Dependent Modulation of the Dynamics of Intracellular Loops Dictates Functional Selectivity of 5-HT2AR. *J. Chem. Inf. Model.* **2022**, *62*, 2522−2537.
(49) Koch, K. W.; Helten, A. Guanylate Cyclase-Based Signaling in Photoreceptors and Retina. In *Signal Transduction in the Retina*; Taylor and Francis, CRC Press, 2008; pp 121−143.
(50) Zägel, P.; Dell'Orco, D.; Koch, K. W. The dimerization domain in outer segment guanylate cyclase is a Ca(2)(+)-sensitive control switch module. *Biochemistry* **2013**, *52*, 5065−5074.
(51) Cudia, D.; Ames, J. Chemical shift assignments of retinal guanylyl cyclase activating protein 5 (GCAP5). *Biomol. NMR Assignments* **2019**, *13*, 201−205.
(52) Peshenko, I. V.; Olshevskaya, E. V.; Lim, S.; Ames, J. B.; Dizhoor, A. M. Calcium-myristoyl Tug. *J. Biol. Chem.* **2012**, *287*, 13972−13984.
(53) Lange, C.; Duda, T.; Beyermann, M.; Sharma, R. K.; Koch, K. W. Regions in vertebrate photoreceptor guanylyl cyclase ROS-GC1 involved in Ca(2+)-dependent regulation by guanylyl cyclase-activating protein GCAP-1. *FEBS Lett.* **1999**, *460*, 27−31.
(54) Laura, R. P.; Hurley, J. B. The kinase homology domain of retinal guanylyl cyclases 1 and 2 specifies the affinity and cooperativity of interaction with guanylyl cyclase activating protein-2. *Biochemistry* **1998**, *37*, 11264−11271.
(55) de Vries, S. J.; van Dijk, M.; Bonvin, A. M. The HADDOCK web server for data-driven biomolecular docking. *Nat. Protoc.* **2010**, *5*, 883−897.
(56) Krylov, D. M.; Hurley, J. B. Identification of proximate regions in a complex of retinal guanylyl cyclase 1 and guanylyl cyclase-activating protein-1 by a novel mass spectrometry-based method. *J. Biol. Chem.* **2001**, *276*, 30648−30654.
(57) Marino, V.; Sulmann, S.; Koch, K. W.; Dell'Orco, D. Structural effects of Mg(2)(+) on the regulatory states of three neuronal calcium sensors operating in vertebrate phototransduction. *Biochim. Biophys. Acta* **2015**, *1853*, 2055−2065.
(58) Senior, A. W.; Evans, R.; Jumper, J.; Kirkpatrick, J.; Sifre, L.; Green, T.; Qin, C.; Zidek, A.; Nelson, A. W. R.; Bridgland, A.; Penedones, H.; Petersen, S.; Simonyan, K.; Crossan, S.; Kohli, P.; Jones, D. T.; Silver, D.; Kavukcuoglu, K.; Hassabis, D. Improved

https://doi.org/10.1021/acs.biochem.4c00046
Biochemistry XXXX, XXX, XXX−XXX

protein structure prediction using potentials from deep learning. *Nature* **2020**, *577*, 706−710.

https://doi.org/10.1021/acs.biochem.4c00046
Biochemistry XXXX, XXX, XXX−XXX